Assembling mechanism of Zr- and other TM-containing polyoxometalates

Pablo Jiménez-Lozano,[a] Albert Solé-Daura,[a] Georges Wipff,[b] Josep M. Poblet,[a] Alain Chaumont,[b] Jorge J. Carbó[*,a]*

[a] Departament de Química Inorgànica i Física, Universitat Rovira i Virgili, Campus Sescelades, Marcel·lí Domingo s/n, 43007 Tarragona, Spain. E-mail: j.carbo@urv.cat

[b] Laboratoire MSM, UMR CNRS 7177, Institut de Chimie, Université de Strasbourg, 1, rue B. Pascal, 6700 Strasbourg, France.

The assembly mechanism of Zr- and other transition metal-substituted polyoxometalates (POMs) to form covalently linked dimers has been analyzed by means of static density functional theory (DFT) calculations with a continuous solvent model as well as Car-Parrinello molecular dynamics (CPMD) simulations with explicit solvent molecules. The study includes different stages of the process: the formation of the active species by alkalination of the solution, and formation of intercluster linkages. CPMD simulations show that the Zr-triaqua precursor, $[W_5O_{18}Zr(H_2O)_3]^{2-}$, at basic conditions, reacts with hydroxide anions to form Zr-aqua-hydro active species, $[W_5O_{18}Zr(OH)(H_2O)]^{3-}$. We computed the DFT potential energy profile for dimerization of $[W_5O_{18}TM(OH)]^{n-}$ (TM = $Zr^{IV}(H_2O)$, Zr^{IV}, Ti^{IV}, and W^{VI}) anions. The resulting overall energy barrier is low for Zr^{IV}, moderate for Ti^{IV}, and high for W^{VI}. The computed

thermodynamic balance favors the dibridged $(\mu OH)_2$ linkages for Zr^{IV}, the monobridged (μOH) linkage for Ti^{IV}, and the monomeric forms for W^{VI}, in agreement with experimentally observed trends. The lowest energy barrier and largest coordination number of Zr-substituted POMs are both a consequence of the flexible coordination environment and larger radius of Zr.

Introduction

Polyoxometalates (POMs) are a well-defined set of anionic molecular transition-metal oxides comprised of Mo, W or V. Their capacity to form a wide variety of clusters, combined with their ability to incorporate other metals, provide them potential applications in many fields including medicine, catalysis, multifunctional materials, chemical analysis, etc.[1,2] These cluster anions can also serve as building blocks for the construction of larger and more complex nanosized architectures, via covalent and noncovalent interactions.[3,4] Nowadays, there is an increasing interest to control these assembly processes to design novel inorganic architectures with new functionalities. The factors that affect the assembly of POMs include a large number of experimental variables such as counterions, concentration of the metal oxide anions, temperature, pH, incorporation of cations or organic ligands, type of heteroatom, and the substituted metal. Among them, the incorporation of heterometallic centers has allowed the condensations of POM structures to form dimeric and other oligomeric units via intercluster linking (Scheme 1).[5] The type of linkage depends strongly on the nature of the incorporated transition metal (TM). Thus, for TM = Nb, Ti, Cr, Fe,[6] the intercluster linkages contain TM-(μO)-TM junctions; for TM = Zr, Hf,[7] the linkages contain TM-$(\mu OH)_2$-TM junctions, whereas for TM = W, Mo and V it is not common to find linkages (see Scheme 1). In agreement with these observations, DFT calculations showed that dimerization is thermodynamically favored for Nb and Ti, while it is

not for V, W, and Mo.[8] In the case of Zr-substituted POMs, we found that the doubly bridged hydroxo structure is thermodynamically more stable than the single bridged oxo structure, in marked contrast with Ti- and Nb-substituted POMs.[9]

Scheme 1

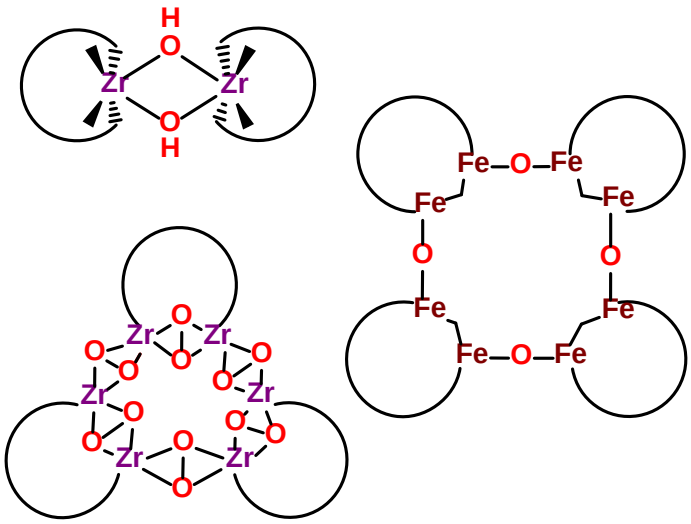

The mechanism of condensation and dimerization reactions involves generally water elimination from two anions at contact distances. Scheme 2 illustrate the proposed mechanism at acidic conditions for A-α-$[SiW_9Nb_3O_{40}]^{7-}$ anions[10] and $[PW_{11}TiO_{40}]^{5-}$ anions.[6d] The acidification can yield the corresponding μ-hydroxo dimer via protonation of the oxo functionality TM=O to form the reactive hydroxo TM-OH group. On the other hand, the Cr-[6g] and Fe-based[6h] dimers are formed from TM-aqua precursor and require the addition of hydroxide. This suggests that under basic conditions the TM-OH_2 group transforms into TM-OH before assembling the POM units as shown in Scheme 2. In the case of Zr-containing POMs, the oligomeric structures have been prepared and isolated from both aqueous and nonaqueous solutions, and at different pH conditions.[9,11,12,13,14,15,16] For example Villannneau et al.[11,12] assembled two Lindqvist monomers by alkalination of Zr-triaqua precursor $(Me_4N)_2[W_5O_{18}Zr(H_2O)_3]$ in aqueous media, whereas

Khodeeva et al.[9] used the "$H_5PW_{11}ZrO_{40}\cdot 14H_2O$" precursor and an excess of TBABr in acidic conditions for POM assembly. Thus, the most probable scenario involves POM assembly through the nucleophilic addition of TM-OH group. Nevertheless, the specific mechanisms of the linkage formation in different conditions, and the final architectures remain to be assessed.

Scheme 2

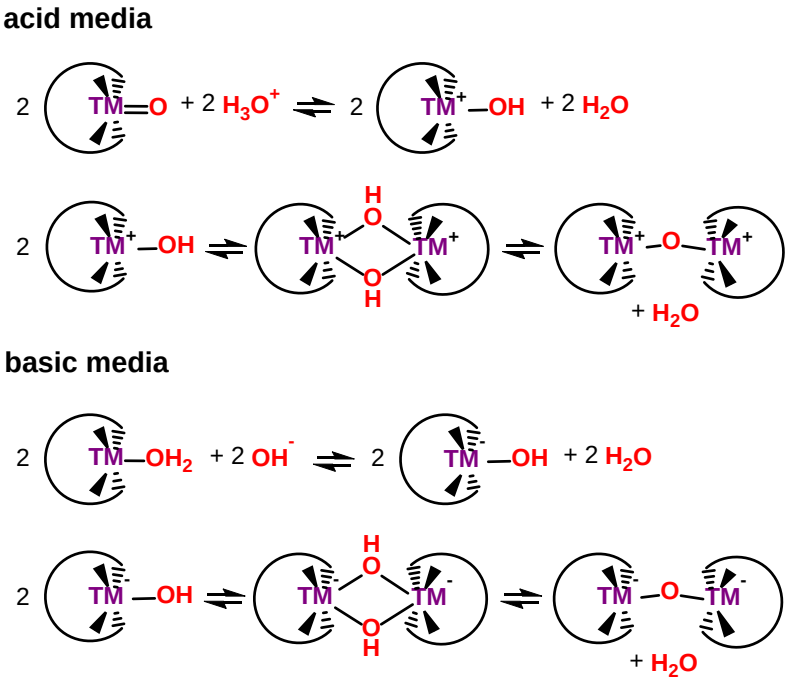

Static DFT calculations studied the thermodynamics of dimerization processes for monosubstitued-Lindqvist and -Keggin anions with different metals.[8,9] More recently in a different context, the dimerization process was examined taking into account the entropy contributions.[17] Mechanistic features involved in the formation of intercluster linkages with a precise characterization of the reactive anionic species and of the intermediates involved remain to be investigated. This is the main focus of this paper. Valuable information of the behavior of POMs in solution can be also obtained from molecular dynamics simulations.[18] In particular, the

collective behavior and aggregation phenomena were studied for non-substituted Keggin-type anions using classical molecular dynamics (MD) simulations.[19,20,21,22] We have used classical MD and Car-Parrinello CPMD simulations with explicit solvent molecules to study the nature of Zr-monosubstituted anions at different pH conditions.[23] In general, the dynamic properties of polyoxometalate anions and analogous polyoxocations have attracted the attention of other authors.[24,25]

Here, we report a detailed study on the assembly mechanism of two Zr-substituted Lindqvist anions, as well as, of other transition metal-substituted anions. The relatively small size of the dimeric system allows us to analyse the process from the generation of the active species up to the formation of the covalent M-μO-M linkages. We employed computational tools to understand at the molecular level the effect of different synthetic parameters such as the pH and the nature of the substituted metal. Firstly, we carry out a CPMD simulations in order to identify the active species of dimeric reaction at the conditions proposed by Villanneau *et al*., namely the alkalination of Zr-triaqua precursor $[W_5O_{18}Zr(H_2O)_3]^{2-}$.[11] Finally, in order to understand the role of the nature of the metal on the reactivity, we determine the key intermediates and transition states (TSs) corresponding to mechanism for different TM-substituted POMs by means of DFT/IEF-PCM calculations.

Methods

DFT calculations. Static calculations were performed with the Gaussian09 package[26] at DFT level by means of the hybrid exchange-correlation B3LYP functional.[27] For Zr, W and Ti atoms, the LANDL2DZ basis set was used.[28] The 6-31G(d,p) basis set[29] was used for the H atoms, as well as for the O atoms of hydroxo ligands, aqua ligands, and directly bound to Zr and Ti. For

the rest of atoms we employed 6-31 G basis set.[29] Solvent effects were included in geometry optimizations by using the IEF-PCM model[30] implemented in Gaussian09.[26] The dielectric constant used for simulate water solvent was ε=78.35. Such a computational level has been successfully employed in the study of the reactivity of group IV-based molecular oxides, yielding quantitative agreement with experimental kinetic parameters.[31] Geometry optimizations of all structures were performed without any symmetry constrains. "Standard" Gibbs free-energies ΔG were first obtained from Gaussian (at 298.15 K and 1 atm) using the default parameters. Free energies were *corrected* ($\Delta G_{corrected}$) using the translational entropy, as developed by Whitesides *et al.*,[32] following the procedure adapted by Sakaki et al.[33] In this approach we used a water concentration of 0.997044 g/cm^3,[34] and molecular volume for water solvent of 25.8×10^{-24} cm^3 per molecule.[35] The employed equations are described in detail in the Supporting Information.

The Whitesides' correction, introduced to study the assembly of multiparticle aggregates, is based on the fact that the volume open to a molecule in a liquid is substantially lower than the total volume, which is the magnitude employed in Sackur-Tetrode equation for translational entropy. The authors defined the volume available to the molecules of a pure liquid as a characteristic *free volume* (V_{free}), which is calculated assuming that the liquid is described by hard cubes.[32] This model representation of the liquid is less accurate for protic solvents, where the network of hydrogen bonds defines also the liquid structure. One could think that the hydrogen bonding increases the density of the liquid, resulting in smaller calculated *free volumes* (for example: V_{free} = 0.028 and 231.495 Å^3 for water and benzene,[33a] respectively). Thus, these small *free volumes* cannot reflect the mobility of the solute in the liquid leading to an overestimation of the Whitesides' correction to translation entropy. In fact, it was recognized that

the approach is less accurate for protic solvents reaching errors that can be greater than 30% in the case of water.[32]

Dynamics simulations. Classical MD simulations were performed using the AMBER11 software[36] in order to generate starting configurations for the CPMD simulations, but also to get some insight into the interaction between the $[W_5O_{18}Zr(H_2O)_3]^{2-}$ and OH^- anions. The parameters for the Zr-substituted POMs were taken from our previous work,[23,37] which followed the procedure by Bonet-Avalos, Bo, Poblet *et al*.[38] (see Supporting Information for further details). Water was represented with the TIP3P model.[39] The 1-4 van der Waals and 1-4 coulombic interactions were scaled down by 2.0. All the simulations were performed with 3D-periodic boundary conditions using an atom-based cutoff of 6 Å for noncovalent interactions and corrected for long-range electrostatic by using particle-particle mesh Ewald (PME) summation method.[40] The simulations were performed at 300 K stating with random velocities. The temperature was monitored by coupling the system to a thermal bath using the Berendsen algorithm[41] with a relaxation time of 0.2 ps. In the NPT simulations, the pressure was similarly coupled to a barostat with a relaxation time of 0.2 ps. A time step of 1 fs was used to integrate the equations of motion via the Verlet leapfrog algorithm.[42] After 500 steps of energy minimization, a 250 ps of dynamics were performed with fixed solutes (BELLY option of AMBER) in order to relax the solvent around the solute. Then, dynamics of 250 ps at constant volume (NVT) followed by 500 ps at a constant pressure (NPT) of 1 atm were carried out. Finally a production run of 1 ns at constant volume was performed.

The CPMD simulations were performed at the DFT level with the CPMD program package.[43] The electronic structure was described by expansion of the valence electronic wave functions into a plane-wave basis set, which is limited by an energy cutoff of 70 Ry. The interaction

between the ionic cores and the valence electrons is treated through the pseudopotential (PP) approximation. Norm-conserving Martins-Troullier PPs are employed.[44] Nonlinear core corrections (NLCC) are employed for W and Cs PP,[45] whereas for Zr a semicore PP was used. We adopted the generalized gradient-corrected BLYP exchange-correlation functional.[27a,46] In the MD simulations, the wave functions are propagated in the Car-Parrinello scheme, by integrating the equations of motion derived from Car-Parrinello Lagrangian.[47] We used a time step of 0.096 fs. A fictitious electronic mass of 900 a.u was employed, and H atoms were substituted by D atoms. The Nosé-Hoover thermostat[48] for the nuclear degrees of freedom was used to maintain the temperature constant around 300 K. The initial geometry was obtained from an equilibrated classical MD simulations of the same system (see above for details). After 0.5 ps of CPMD equilibration, the production run was performed.

Results and discussion

In a step forward with respect to the previous studies on POM dimerization,[8,9,23] we performed a computational study of the assembling mechanism of Zr- and other TM-containing POMs that includes the analysis of the nature of the active species at a given pH, the mechanism of formation of intercluster linkages, and the effect of the nature of substituted metal. As a reference we selected the system and the reaction conditions reported by Villanneau *et al*.,[12] who obtained the $(Me_4N)_6[\{W_5O_{18}Zr(\mu\text{-}OH)\}_2]\cdot(H_2O)_2$ dimer in aqueous conditions by alkalination of the corresponding Zr-aqua precursor $(Me_4N)_2[W_5O_{18}Zr(H_2O)_3]$. The relatively simple POM structure allowed us to use computationally demanding calculations such as CPMD simulations and DFT determination of reaction intermediates and transition states.

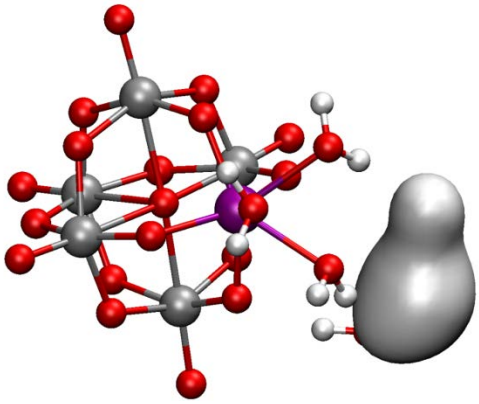

Figure 1. $[W_5O_{18}Zr(H_2O)_3]^{2-}$ anion in basic solution, simulated by classical MD (20 ns). The highest density region of the $O(OH^-)$ atom is marked in grey.

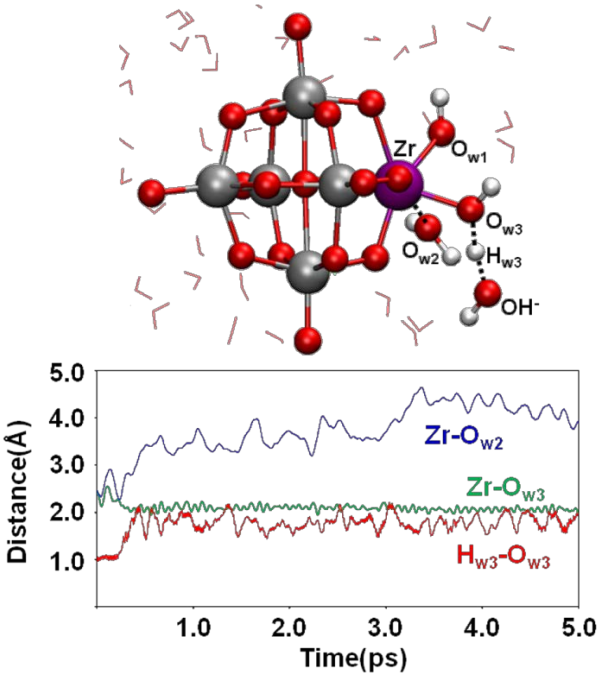

Figure 2. Evolution of selected Zr-O and O(aqua)-H distances (in Å) during 5 ps of CPMD simulation at basic conditions, starting from the $[W_5O_{18}Zr(H_2O)_3]^{2-}$ anion. A snapshot illustrates the H transfer to OH^-, coupled with aqua ligand decoordination, to yield the $[W_5O_{18}Zr(OH)(H_2O)]^{3-}$ anion.

CPMD simulations on the $[W_5O_{18}Zr(H_2O)_3]^{2-}$ precursor in basic conditions. To identify the nature of the reactive monomeric species involved in dimerization, we surrounded the $[W_5O_{18}Zr(H_2O)_3]^{2-}$ anion by 129 water molecules, 1 OH^- and 3 Cs^+ to neutralize the solution, as in the experimental study by Villanneau *et al.*[12] An initial classical MD simulation provided interesting insights into the non-covalent interactions between OH^- and the protons of $Zr(OH_2)$ ligands. During the first 8.8 ns of simulation, OH^- showed a Brownian movement. Then, it became hydrogen-bonded to one of the $Zr(OH_2)$ protons. This type of interaction survived for the rest of the simulation (20 ns), in which OH^- jumped between two aqua ligands. We cannot discard that the OH^- interacts with the third aqua ligand if longer simulation times were available. Figure 1 depicts the density of the $O(OH^-)$ atom, which is clearly highest around the $Zr(OH_2)$ moieties.

As a starting point for a 5-ps CPMD simulation, we used a structure where the hydroxide anion forms a hydrogen-bond with one of three aqua ligands. To evaluate the reaction events, we plot in Figure 2 the evolution of distances $Zr\text{-}O_{w2}$, $Zr\text{-}O_{w3}$ and $O_{w3}\text{-}H_{w3}$ along 5-ps. Figure 2 also shows a snapshot where a key event of the simulation is observed. After 0.22 ps of simulation, one proton of the aqua ligand is transferred to the hydroxide anion to form the corresponding Zr-hydroxo group. Simultaneously, one of the aqua ligands decoordinates from the Zr center, as reflected on the increase of $Zr\text{-}O_{w2}$ distance, yielding the more stable hydroxo-aqua $[W_5O_{18}Zr(OH)(H_2O)]^{3-}$ species. This new species remained stable during the rest of the simulation. This is consistent with previous CPMD studies where the $Zr\text{-}OH_2$ groups transformed into Zr-OH in basic conditions.[23] In the light of these findings and the tendency of Zr to be 7- or 8-fold coordinated, we propose that upon alkalination, the Zr-triaqua POM converts into an aqua-hydroxo species. Thus, in the next sections, we will use the

$[W_5O_{18}Zr(OH)(H_2O)]^{3-}$ anion as the reactive species in the formation of the Zr-μO(H)-Zr linkages. It will also be compared to its dehydrated form $[W_5O_{18}Zr(OH)]^{3-}$.

The formation of the covalent linkages. We characterized the formation of the covalent Zr-$\mu(OH)_2$-Zr bonds by determining the corresponding transition states at the B3LYP level, in conjunction with continuum IEF-PCM model to account for solvent effects of water. Figure 3 displays the computed free energy profile for the assembly of two Zr-hydroxo-aqua $[W_5O_{18}Zr(OH)(OH_2)]^{3-}$ (**1l-H_2O**) anions, and Figure 4 shows the molecular structures of the most relevant species. Since calculated Gibbs free energies overestimate the translational entropy loss in the associative processes, we corrected them by applying Whitesides' correction[32] and reported the new values in parenthesis. It is important to note that the entropy correction is less accurate for protic solvents, and specially, for water (see the Methods sections for detailed discussion).[32] Overall, the combination of corrected and uncorrected values is informative because it provides a lower and an upper limit of entropy loss in associative processes such as the dimerizations studied here.

We could locate, within a narrow range of energies, several non-covalently bound dimers, in which the shortest Zr···Zr distance is 4.58 Å, and the two monomers are linked in different ways via hydrogen bonds. Structure **2l-H_2O** shows three hydrogen bonds with the following patterns: 1) between an aqua ligand hydrogen and a hydroxo ligand oxygen ($H_w\cdots O_h$), 2) between an aqua ligand hydrogen and a bridging Zr-O-W oxygen ($H_w\cdots O_b$), and 3) between a hydroxo ligand hydrogen and a bridging Zr-O-W oxygen ($H_h\cdots O_b$). Its computed free-energy is 5.3 kcal·mol^{-1} above reactants; however, upon introduction of entropy correction the computed value becomes

0.7 kcal·mol^{-1} below the reactants. Thus, the hydrogen bond formation between POMs compensates their coulombic repulsion, which can be easily overcome at room temperature.

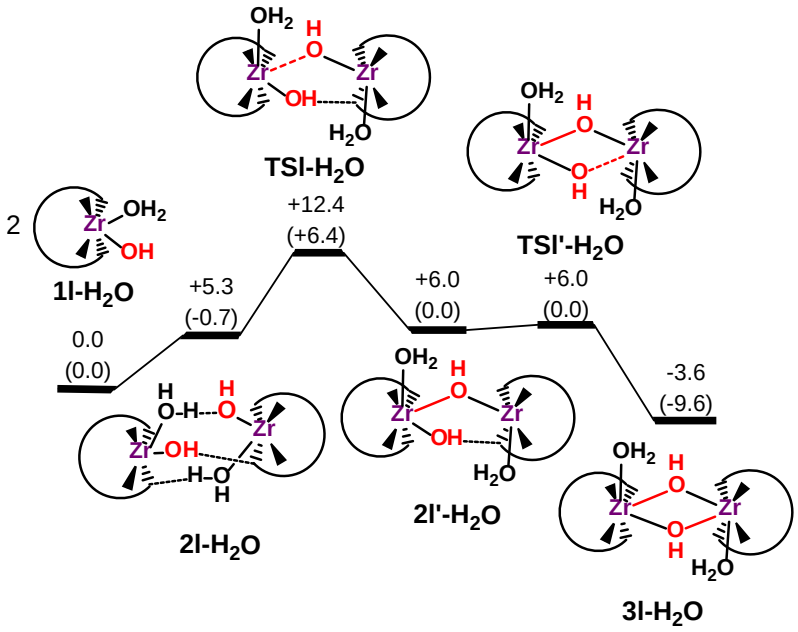

Figure 3. Calculated free energy profile for the assembly of two $[W_5O_{18}Zr(OH)(H_2O)]^{3-}$ anions. The relative free energies (kcal.mol^{-1}) without and with Whitesides' correction (in parenthesis).

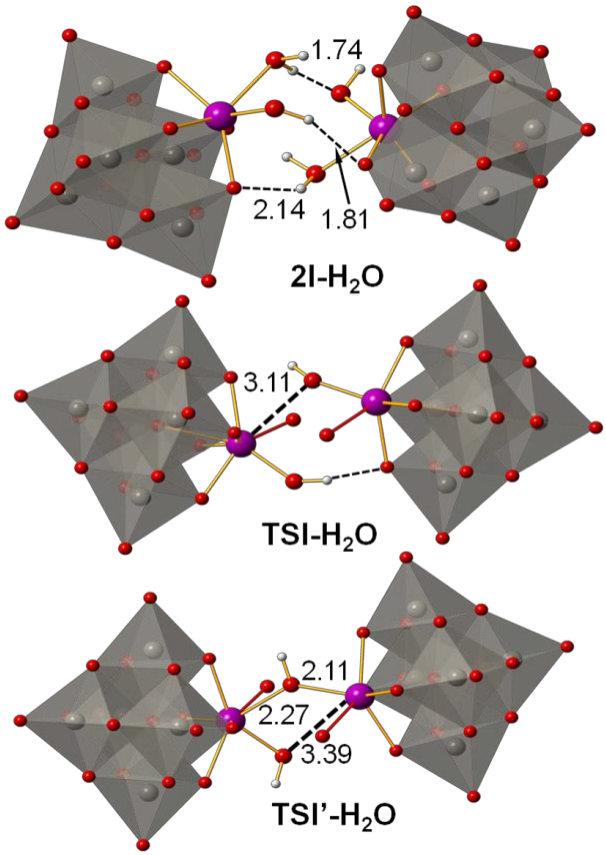

Figure 4. DFT structures and main distances (in Å) for hydrated Lindqvist structures, **2l-H_2O**, **TSl-H_2O** and **TSl'-H_2O**. The hydrogen atoms of the aqua ligands have been omitted for clarity in transition state structures.

From the adduct **2l-H_2O**, the formation of the two Zr-μO(H)-Zr linkages to obtain the covalently bound dimer **3l-H_2O** proceeds in two steps (Figure 3). Along the process the Zr···Zr distance decreases continuously from 4.58 Å in **2l-H_2O** to 3.69 Å in **3l-H_2O** (see Table-S1). In between, we located an intermediate, **2l'-H_2O**, which can be defined as a μ-monohydroxo dimer containing the Zr moiety {(H_2O)Zr-(μ-OH)-Zr(OH)(OH_2)}, with Zr-(μ-OH) distances of 2.15 and 2.54 Å, respectively. The **2l'-H_2O** structure sits at +6.0 kcal·mol^{-1} above the reactants (or it is isoenergetic with the Whitesides' correction). In the first TS, **TSl-H_2O**, the Zr···O(H) distance

of the forming bond is 3.11 Å, while the other Zr···O(H) distance (3.66 Å) is longer, but shorter than in non-covalent dimer **2l-H_2O** (4.06 Å). This indicates that the first free energy barrier corresponds to the bridging bond-forming process. The computed free-energy barrier for the first Zr-O formation from **2l-H_2O** is low, +7.1 kcal·mol^{-1}.[49] As in **2l-H_2O**, the **TSl-H_2O** structure shows three intercluster hydrogen bonds: two between the aqua ligands and the Zr-O-W oxygens ($H_w\cdots O_b$), and one between the hydroxo ligand and a Zr-O-W oxygen ($H_h\cdots O_b$). The second TS, **TSl'-H_2O**, connects the **2l'-H_2O** intermediate with the μ-dihydroxo dimer $[\{W_5O_{18}Zr(OH_2)(\mu\text{-}OH)\}_2]^{6-}$ (**3l-H_2O**). The computed energy barrier is very low and it becomes zero when we introduce thermal and entropic corrections. This indicates that **2l'-H_2O** intermediate is a very shallow minimum and its existence in the potential energy profile could depend on the specific reaction conditions. The whole process is exergonic by 3.6 kcal·mol^{-1} (or 9.6 kcal·mol^{-1} with the Whitesides' correction) and the global free-energy barrier (12.4 kcal·mol^{-1} and 7.1 kcal·mol^{-1} after correction) is modest. Thus, once a non-covalent dimer like **2l-H_2O** is formed, rearrangement to dimeric structures with covalent linkages Zr-(μ-$OH)_2$-Zr is thermodynamically favorable, and presumably, a fast process in solution.

We also considered an alternative "dissociative" mechanism, which starts with the decoordination of the aqua ligand from two **1l-H_2O** units, yielding the non-hydrated species $[W_5O_{18}Zr(OH)]^{3-}$ (**1l**) prior to formation of the linkages (Figure 5). Then, subsequent recoordination of water to the Zr centers could lead to the hydrated dimer **3l-H_2O**. We previously computed that the dehydration of $[W_5O_{18}Zr(H_2O)(OH)]^{3-}$ (**1l-H_2O**) is endothermic by +11.3 kcal·mol^{-1} in terms of electronic energy.[23] However, when accounting for entropic effects, the dehydration process becomes either favorable (ΔG = -1.9 kcal·mol^{-1} per unit) or, at least, less unfavorable ($\Delta G_{corrected}$ = +4.1 kcal·mol^{-1} per unit). Two non-hydrated $[W_5O_{18}Zr(OH)]^{3-}$ species

(**1l**) can then form a non-covalent adduct (**2l**) via hydrogen bonding between the Zr(OH) protons and the basic oxygens of POM framework. The formation of **2l** is slightly less favorable than the one of **2l-H_2O** (ΔG(**1**→**2**) = +8.0 *vs.* +5.3 kcal·mol^{-1}, and $\Delta G_{corrected}$(**1**→**2**) = +2.0 *vs.* -0.7 kcal·mol^{-1}), in keeping with the lessened number of bridging H-bonds in **2l**, compared to **2l-H_2O**. However, the computed value is still low enough to assume that the coulombic repulsion between the -3 charged anions can be overcome under experimental conditions.

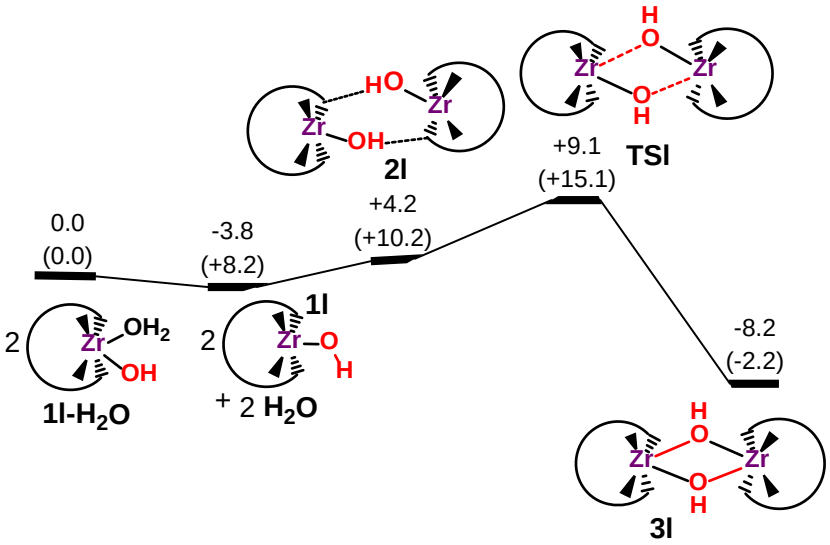

Figure 5. Calculated free energy profile for the dimerization of two $[W_5O_{18}Zr(OH)(H_2O)]^{3-}$ anions **1l** ("dissociative" mechanism). The relative free energies and Whitesides' corrected free energies (in parenthesis) are given in kcal·mol^{-1}.

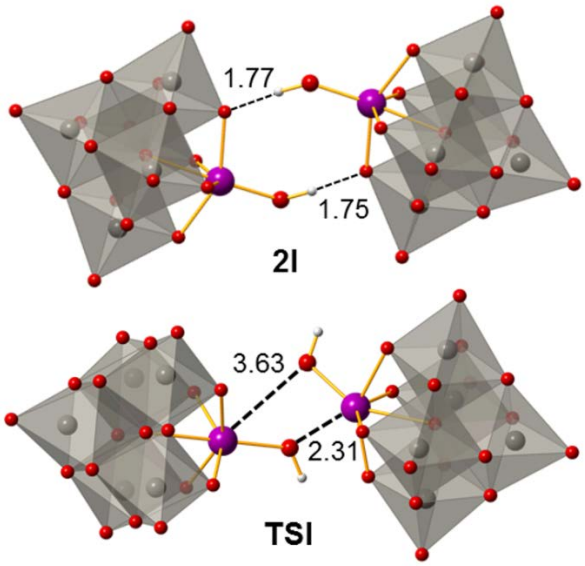

Figure 6. DFT structures and main distances (in Å) for nonhydrated Lindqvist structures, **2l** and **TSl**.

The main difference between the "dissociative" and "hydrated" mechanisms is that in the former we only found one TS (**TSl**), in which the two Zr···O bonds are formed in a concerted, yet asynchronous way. Indeed, the geometry of **TSl** shows distinct distances for the Zr-μOH forming bonds: 2.31 and 3.63 Å, respectively (see Figure 6). From the **2l** non-covalent dehydrated dimer, the computed free energy barrier (4.9 kcal·mol^{-1})[49] is very low. In fact, the barrier is even lower than that for the hydrated system (7.1 kcal·mol^{-1}), probably because the larger flexibility of the unsaturated Zr centers can accommodate more easily the additional bridging ligands. The resulting non-hydrated dimer, **3l**, has an energy below the two monomers **1l**. As can be observed in Figure 5, the computed overall energy barrier is 12.9 kcal·mol^{-1} for the **1l** → **TSl** transformation, or $\Delta G^{\neq}_{corrected}$ = 15.1 kcal·mol^{-1} after entropy corrections for the **1l-H_2O** → **TSl** transformation. It is difficult to answer definitely whether the "dissociative" or the "hydrated" mechanism is least energetically demanding because of the small energy differences observed

and of the difficulties to evaluate entropic contributions in solution for processes with different molecularities. Nevertheless, the calculations indicate that the "hydrated" mechanism could be slightly favored in aqueous media: the estimated overall barriers without and with entropy corrections are respectively 12 and 7 kcal·mol^{-1} for the "hydrated" mechanism and 13 and 15 kcal·mol^{-1} for the "dissociative" one.

In order to assess the effect of the size and charge of the anionic monomer, we additionally evaluated the main steps of the dimerization of the corresponding Keggin anion $[PW_{10}O_{39}Zr(OH)]^{4-}$ (**1k**). Table 1 compares the free-energy values for **1k** with those of Lindqvist species **1l** and **1l-H_2O**, while Figure S1 shows the molecular structures of the Keggin dimers. The formation of the hydrogen bonded adduct **2k** is thermodynamically less favorable than for the corresponding Lindqvist structure **2l**, due to the higher negative charge of the Keggin anions. When compared to the hydrated dimer **2l-H_2O**, the energy difference becomes even larger, because **2k** can establish only two, instead of three hydrogen bonds. Likewise, the free-energy barrier for the formation of covalent linkages is somewhat higher for the Keggin anions **1k** (by ~2 kcal·mol^{-1}) than for the corresponding Lindqvist anions **1l**. Nevertheless, the results for Keggin anions are qualitatively very similar to those of Lindqvist, and consequently, it is reasonable to think that the "hydrated" mechanism and the pH dependence on the formation of the active species for **2k-H_2O** anions, as well as other Zr-containing anions, is very similar to those characterized for Lindqvist anions.

Table 1. Main energetic parameters of the dimerization process of two $[W_5O_{18}Zr(H_2O)_n(OH)]^{3-}$ or $[PW_{10}O_{39}Zr(OH)]^{4-}$ anions.[a)]

compound	**ΔG (1→2)**	**$\Delta G^{\neq}$ (2→TS)**
$[W_5O_{18}Zr(H_2O)(OH)]^{3-}$ (**1l-H_2O**)	+5.3 (-0.7)	7.1
$[W_5O_{18}Zr(OH)]^{3-}$ (**1l**)	+8.0 (+2.0)	4.9
$[PW_{10}O_{39}Zr(OH)]^{4-}$ (**1k**)	+10.1 (+4.0)	7.2

a) Values in parenthesis represent corrected free energies. All energies are in kcal·mol^{-1}.

The effect of the TM nature. Scheme 3 shows the possible species involved in the assembly process for several transition metal-substituted Lindqvist anions. Table 2 collects relevant energetic parameters computed for different transition metals (TM = W(VI), Ti(IV), and Zr(IV)). In the studied series, the W(VI) anion forms the strongest non covalent adduct and the Zr(IV) one the weakest (ΔG(**1**→**2**) = -10.9 and +8.0 kcal·mol^{-1}, respectively; $\Delta G_{corrected}$(**1**→**2**) = -16.9 and +4.0 kcal·mol^{-1}, respectively). We observe a clear correlation between the magnitude of the POM charge and the strength of the non-covalent binding: the lower the charge, the stronger the interaction is: the ΔG_{adduct}(**1**→**2**) interaction energies follow the order: W(VI) > Ti (IV) > Zr(IV). Note also that the type of transition-metal not only determines the total anionic charge. It also influences the strength of the intermolecular hydrogen bonds between the TM-OH protons and the TM-O-W bridging oxygens.

The computed free energy barriers for the formation of the dibridged dimer **3** from adduct **2** ($\Delta \mathbf{G}^{\neq}$(**2**→**TS**)) follow trends in agreement with observations. The highest barrier (> 35 kcal·mol^{-1}) corresponds to W(VI), for which covalent assembly never happens. On the other hand, Ti(IV) and Zr(IV), which form intercluster linkages, have lower free energy barriers (< 25 kcal·mol^{-1}).

Interestingly, the energy barrier for Zr-substituted POM is significantly lower than that of Ti-substituted POM, carrying both the same charge. This behavior is easy to rationalize recalling the larger atomic radius of Zr compared to Ti. The biggest atom provides a more flexible center to bend the hydroxo ligand and to coordinate an additional atom in order to form the dibridged species. Finally, the thermodynamics of dimer formation follows the same trends found in our previous contributions.[8,9]

Scheme 3

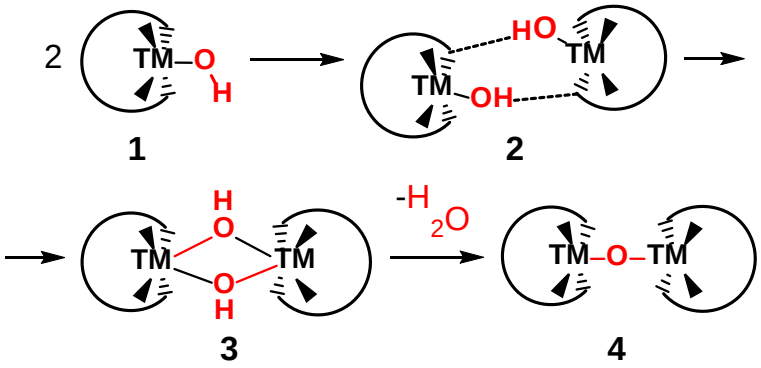

Table 2. Free energy comparison of key steps in the assembly process for $[W_5O_{18}TM(OH)]^{n-}$ (TM = W, Ti and Zr) and for $[W_5O_{18}Zr(OH)(H_2O)]^{3-}$ anions.[a)]

TM	ΔG(1→2)	$\Delta G^{\neq}$(2→TS)	ΔG (1→3)	ΔG (1→4)
W(VI)	-10.9 (-16.9)	38.2	+20.1 (+14.1)	+10.6
Ti(IV)	+2.7 (-3.3)	24.5	+23.3 (+17.3)	-0.7
Zr(IV)H_2O	+5.3 (-0.7)	7.1	-3.6 (-9.6)	-
Zr(IV)	+8.0 (+2.0)	4.1	-4.4 (-10.4)	+4.9

a) Values in parenthesis represent corrected free energies. All energies are in kcal·mol^{-1}.

Conclusions

We have studied mechanistic features of the assembly mechanism of Zr- and other metal substituted POMs into dimeric clusters. To this end, we have employed static DFT methods and CPMD simulations that allowed us to assess the effects of pH and metal nature CPMD simulations on the $[W_5O_{18}Zr(H_2O)_3]^{2-}$ precursor in aqueous basic media showed that the Zr-OH_2 groups transform into Zr-OH groups. The resulting Zr-hydroxo-aqua anion, $[W_5O_{18}Zr(OH)(H_2O)]^{3-}$, is the most likely active species for the assembly process. Dimerization occurs through the stepwise formation of two covalent Zr-μO(H)-Zr linkages, for which the computed overall free energy barrier is low (12.4 and 7.1 kcal·mol^{-1} for $\Delta G^{\neq}$ and $\Delta G^{\neq}_{corrected}$, respectively). The nature of the addenda ion is crucial to the assembly and to define the type of intercluster linkage: the computed energy barriers follow the order: W(VI) > Ti (IV) > Zr(IV). For TM = W(VI), for which covalent assembly never happens, the barrier is the highest (> 35 kcal·mol^{1}), whereas for Ti(IV) and Zr(IV), which form intercluster linkages, the barriers are lower (< 25 kcal·mol^{-1}). Within the studied series of metals, the Zr shows the lowest energy barrier, as a dual consequence of its low charge and its flexible coordination environment.

ASSOCIATED CONTENT

Supporting Information. Additional computational details, additional structure representations and geometric parameters, and xyz coordinates for the most relevant structures

AUTHOR INFORMATION

Corresponding Author

*E-mails: j.carbo@urv.cat

ACKNOWLEDGMENT

Research at was supported by the Spanish Ministry of Science and Innovation (CTQ2014-52774-P) and the Generalitat de Catalunya (2014SGR199 and XRQTC).

References

1. *Chemical Society Reviews*, ed. Cronin, L.; Müller, A. 2012, vol. 41, 7325.

2. (a) Proust, A.; Thouvenot, R.; Gouzerh, P. Functionalization of polyoxometalates: towards advanced applications in catalysis and materials science *Chem. Commun.* **2008**, 1837; (b) Mizuno N.; Yamaguchi, K. Polyoxometalate catalysts: toward the development of green H_2O_2-based epoxidation systems *Chem. Rec.* **2006**, *6*, 12; (c) *Chemical Reviews*, ed. Hill, C. L., 1998, vol. 98.

3. (a) Miras, H.; Yan, J.; Long, D. L.; Cronin, L. Engineering polyoxometalates with emergent properties *Chem. Soc. Rev.* **2012**, *41*, 7403; (b) Long, D. L.; Tsunashima, R.; Cronin, L. Polyoxometalates: Building Blocks for Functional Nanoscale Systems *Angew. Chem., Int. Ed.* **2010**, *49*, 1736; (c) Mothé-Esteves, P.; Marciel-Pereira, M.; Arichi, J.; Louis, B. How Keggin-Type Polyoxometalates Self-Organize into Crystals *Crystal Growth & Design* **2010**, *10*, 371; (d) Nisar, A.; Lu, Y.; Wang, X. Assembling Polyoxometalate Clusters into Advanced Nanoarchitectures *Chem. Mater.* **2010**, *22*, 3511; (e) Müller, A.; Diemann, E.; Kuhlmann, C.; Eimer, W.; Sarain, C.; Tak, T.; Knöchel, A.; Pranzas, P. K. Hierarchic patterning: architectures beyond‘giant molecular wheels’ *Chem. Commun.* **2001**, 1928.

4. Winter, R. O.; Cameron, J. M.; Cronin, L. Controlling the Minimal Self Assembly of “Complex” Polyoxometalate Clusters *J. Am. Chem. Soc.* **2014**, *136*, 12753.

5. Oms, O.; Dolbecq, A.; Milane, P. Diversity in structures and properties of 3d-incorporating polyoxotungstates *Chem. Soc. Rev.* **2012**, *41*, 7497.

6. See for example: (a) Finke, R. G.; Droege, M. W. Trisubstituted heteropolytungstates as soluble metal oxide analogs. 1. The preparation, characterization, and reactions of organic solvent soluble forms of the silicon-niobium heteropolytungstates $Si_2W_{18}Nb_6O_{77}^{8-}$, $SiW_9Nb_3O_{40}^{7-}$, and the $SiW_9Nb_3O_{40}^{7-}$ supported organometallic complex $[(C_5Me_5)Rh.cntdot.SiW_9Nb_3O_{40}]^{5-}$ *J. Am. Chem. Soc.* **1984**, *106*, 7274; (b) Day, V. W.; Klemperer, W. G.; Schwartz, C. Synthesis, characterization, and interconversion of the niobotungstic acid $Nb_2W_4O_{19}H^{3-}$ and its anhydride and alkyl/silyl esters *J. Am. Chem. Soc.* **1987**, *109*, 6030; for Keggin and Lindqvist dimers with TM = Nb; (c) Lin, Y.; Weakley, T. J. R.; Rapko, B.; Finke, R. G. Polyoxoanions derived from tungstosilicate (A-.beta.-$SiW_9O_{34}^{10-}$): synthesis, single-crystal structural determination, and solution structural characterization by tungsten-183 NMR and IR of titanotungstosilicate (A-.beta.-$Si_2W_{18}Ti_6O_{77}^{14-}$) *Inorg. Chem.* **1993**, *32*, 5095; (d) Kholdeeva, O. A.; Maksimov, G. M.; Maksimovskaya, R. I.; Kovaleva, L. A.; Fedotov, M. A.; Grigoriev, V. A.; Hill, C. L. Dimeric Titanium-Containing Polyoxometalate. Synthesis, Characterization, and Catalysis of H_2O_2-Based Thioether Oxidation *Inorg. Chem.* **2000**, *39*, 3828; (e) Errington, R. J.; Petkar, S. S.; Middleton, P. S.; McFarlene, W.; Clegg, W.; Coxall, R. A.; Harrington, R. W. Non-aqueous synthetic methodology for TiW_5 polyoxometalates: protonolysis of $[(MeO)TiW_5O_{18}]^{3-}$ with alcohols, water and phenols *Dalton Trans.* **2007**, 5211; (f) Matsuki, Y.; Mouri, Y.; Sakai, Y.; Matsunaga, S.; Nomiya, K. Monomer and Dimer of Mono-titanium(IV)-Containing α-Keggin Polyoxometalates: Synthesis, Molecular Structures, and pH-Dependent Monomer–Dimer Interconversion in Solution *Eur. J. Inorg. Chem.* **2013**, 1754; for Keggin and Lindqvist dimers with TM = Ti; (g) Wassermann, K.; Palm, R.; Lunk, H. J.; Fuchs, J.; Steinfeldt, N.; Stösser, R.

Condensation of Keggin Anions Containing Chromium(III) and Aluminum(III), Respectively. 1. Synthesis and X-ray Structural Determination of [{A-.alpha.-$SiO_4W_9O_{30}(OH)_3Cr_3$}$_2$$(OH)_3$]$^{11-}$ *Inorg. Chem.* **1995**, 5029; for Keggin dimers with TM = Cr; (h) Zonnevijlle, F.; Tourné, C. M.; Tourné, G. F. Preparation and characterization of iron(III)- and rhodium(III)-containing heteropolytungstates. Identification of novel oxo-bridged iron(III) dimers *Inorg. Chem.* **1982**, *21*, 2751; (i) Bi, L. H.; Kortz, U.; Nellutla, S.; Stowe, A. C.; van Tol, J.; Dalal, N. S.; Keita, B.; Nadjo, L. Structure, Electrochemistry, and Magnetism of the Iron(III)-Substituted Keggin Dimer, [$Fe_6(OH)_3$(A-α-$GeW_9O_{34}(OH)_3)_2$]$^{11-}$ *Inorg. Chem.* **2005**, *44*, 896; (j) Santos, F. M.; Brandao, P.; Félix, V.; Rosário, M.; Domingues, M.; Amaral, J. S.; Amaral, V. S.; Nogueira, H. I. S.; Cavaleiro, A. M. V. Organic–inorganic hybrid materials based on iron(III)-polyoxotungstates and 1-butyl-3-methylimidazolium cations *Dalton Trans.* **2012**, *41*, 12145; for Keggin dimers with TM = Fe.

7. (a) Osada, H.; Ishikawa, A.; Saku, Y.; Sakai, Y.; Matsuki, Y.; Matsunga, S.; Nomiya, K. 2:2-Type complexes of zirconium(IV)/hafnium(IV) centers with mono-lacunary Keggin polyoxometalates: Syntheses and molecular structures of [(α-$SiW_{11}O_{39}M)_2(\mu$-$OH)_2$]$^{10-}$ (M = Zr, Hf) with edge-sharing octahedral units and [(α-$SiW_{11}O_{39}M)_2(\mu$-$OH)_3$]$^{11-}$ with face-sharing octahedral units *Polyhedron* **2013**, *52*, 389; (b) Nomiya, K.; Sakai, Y.; Matsunaga, S. Chemistry of Group IV Metal Ion-Containing Polyoxometalates *Eur. J. Inorg. Chem.* **2011**, 179, and references therein.

8. López, X.; Weinstock, I. A.; Bo, C.; Sarasa, J. P.; Poblet, J. M. Structural Evolution in Polyoxometalates: A DFT Study of Dimerization Processes in Lindqvist and Keggin Cluster Anions *Inorg. Chem.* **2006**, *45*, 6467

9. Kholdeeva, O. A.; Maksimov, G. M.; Maksimovskaya, R. I.; Vanina, M. P.; Trubitsina, T. A.; Naumov, D. Y.; Kolesov, B. A.; Antonova, N. S.; Carbó, J. J.; Poblet, J. M. Zr^{IV}-Monosubstituted Keggin-Type Dimeric Polyoxometalates: Synthesis, Characterization, Catalysis of H_2O_2-Based Oxidations, and Theoretical Study *Inorg. Chem.* **2006**, *45*, 7224.

10. Kim, G. S.; Zeng, H.; Neiwert, W. A.; Cowan, J. J.; van Derveer, D.; Hill, C. L.; Weinstock, I. A. Dimerization of A-α-$[SiNb_3W_9O_{40}]^{7-}$ by pH-Controlled Formation of Individual Nb−μ-O−Nb Linkages *Inorg. Chem.* **2003**, *42*, 5537.

11. Villanneau, R.; Carabineiro, H.; Carrier, X.; Thouvenot, R.; Herson, P.; Lemos, F.; Ramôa-Ribeiro, F.; Che, M. Synthesis and Characterization of Zr(IV) Polyoxotungstates as Molecular Analogues of Zirconia-Supported Tungsten Catalysts *J. Phys. Chem. B* **2004**, *108*, 12465.

12. Carabineiro, H.; Villanneau, R.; Carrier, X.; Herson, P.; Lemos, F.; Ramôa Ribeiro, F.; Proust, A.; Che, M. Zirconium-Substituted Isopolytungstates: Structural Models for Zirconia-Supported Tungsten Catalysts *Inorg. Chem.* **2006**, *45*, 1915.

13. Errington, R. J.; Petkar, S. S.; Middleton, P. S.; McFarlane, W.; Clegg, W., Coxall, R. A.; Harrington, R. W. Synthesis and Reactivity of the Methoxozirconium Pentatungstate $(^nBu_4N)_6[\{(\mu\text{-}MeO)ZrW_5O_{18}\}_2]$: Insights into Proton-Transfer Reactions, Solution Dynamics, and Assembly of $\{ZrW_5O_{18}\}^{2-}$ Building Blocks *J. Am. Chem. Soc.* **2007**, 129, 12181.

14. Nomiya, K.; Saku, Y.; Yamada, S.; Takahashi, W.; Sekiya, H.; Shinohara, A.; Ishimaru, M.; Sakai, Y. Synthesis and structure of dinuclear hafnium(IV) and zirconium(IV) complexes sandwiched between 2 mono-lacunary α-Keggin polyoxometalates *Dalton Trans.* **2009**, 5504.

15. Yamaguchi, S.; Kikukawa, Y.; Tsushida, K.; Nakagawa, Y.; Uehara, K.; Yamaguchi, K.; Mizuno, N. Synthesis and Structural Characterization of a γ-Keggin-Type Dimeric Silicotungstate with a Bis(μ-hydroxo) Dizirconium Core $[(\gamma\text{-}SiW_{10}O_{36})_2Zr_2(\mu\text{-}OH)_2]^{10-}$ *Inorg. Chem.* **2007**, *46*, 8502; (b) Kikukawa, Y.; Yamaguchi, S.; Tsuchida, K.; Nakagawa, Y.; Uehara, K.; Mizuno, N. Synthesis and Catalysis of Di- and Tetranuclear Metal Sandwich-Type Silicotungstates $[(\gamma\text{-}SiW_{10}O_{36})_2M_2(\mu\text{-}OH)_2]^{10-}$ and $[(\gamma\text{-}SiW_{10}O_{36})_2M_4(\mu_4\text{-}O)(\mu\text{-}OH)_6]^{8-}$ (M = Zr or Hf) *J. Am. Chem. Soc.* **2008**, *130*, 5472.

16. Saku, Y.; Sakai, Y.; Nomiya, K. Relation among the 2:2-, 1:1- and 1:2-type complexes of hafnium(IV)/zirconium(IV) with mono-lacunary α_2-Dawson polyoxometalate ligands: Synthesis and structure of the 2:2-type complexes $[\{\alpha_2\text{-}P_2W_{17}O_{61}M(\mu\text{-}OH)(H_2O)\}_2]^{14-}$ (M = Hf, Zr) *Inorg. Chim. Acta* **2010**, *363*, 967.

17. Loung, T. K. N.; Shestakova, P.; Mihaylov, T. T.; Absillis, G.; Pierloot, K.; Parac-Vogt, T. N. Multinuclear Diffusion NMR Spectroscopy and DFT Modeling: A Powerful Combination for Unraveling the Mechanism of Phosphoester Bond Hydrolysis Catalyzed by Metal-Substituted Polyoxometalates *Chem. Eur. J.* **2015**, *21*, 4428.

18. (a) López, X.; Miró, P.; Carbó, J. J.; Rodríguez-Fortea, A.; Bo, C.; Poblet, J. M. Current trends in the computational modelling of polyoxometalates *Theor. Chem. Acc.* **2011**, *128*, 393; (b) López, X.; Carbó, J. J.; Bo, C.; Poblet, J. M. Structure, properties and reactivity of polyoxometalates: a theoretical perspective *Chem. Soc. Rev.* **2012**, *41*, 7537.

19. (a) Chaumont, A.; Wipff, G. Ion aggregation in concentrated aqueous and methanol solutions of polyoxometallates Keggin anions: the effect of counterions investigated by molecular dynamics simulations *Phys. Chem. Chem. Phys.* **2008**, *10*, 6940; (b) Chaumont, A.;

Wipff, G. Polyoxometalate Keggin Anions at Aqueous Interfaces with Organic Solvents, Ionic Liquids, and Graphite: a Molecular Dynamics Study *J. Phys. Chem. C* **2009**, *113*, 18233.

20. (a) Chaumont, A.; Wipff, G. Do Keggin anions repulse each other in solution? The effect of solvent, counterions and ion representation investigated by free energy (PMF) simulations. *C. R. Chim.* **2012**, *15*, 107; (b) Chaumont, A.; Wipff, G. Interactions between Keggin Anions in Water: The Higher Their Charge, the Higher Their Condensation? A Simulation Study *Eur. J. Inorg. Chem.* **2013,** 1835.

21. Bera, M. K.; Qiao, B.; Seifert, S.; Burton-Pye, B. P.; de la Cruz, M. O.; Antonio, M. R. Aggregation of Heteropolyanions in Aqueous Solutions Exhibiting Short-Range Attractions and Long-Range Repulsions *J. Phys. Chem. C*, **2016**, *120*, 1317.

22. Serapian, S. A.; Bo, C. Simulating the Favorable Aggregation of Monolacunary Keggin Anions *J. Phys. Chem. B,* **2016**, *120*, 12959.

23. Jiménez-Lozano, P., Carbó, J. J., Chaumont, A., Poblet, J. M., Rodriguez-Fortea, A., Wipff, G. Nature of Zr-Monosubstituted Monomeric and Dimeric Polyoxometalates in Water Solution at Different pH Conditions: Static Density Functional Theory Calculations and Dynamic Simulations *Inorg. Chem.* **2014**, *53*, 778.

24. (a) Rustad, J. R.; Casey, W. H. Metastable structures and isotope exchange reactions in polyoxometalate ions provide a molecular view of oxide dissolution *Nat. Mat.* **2012**¸*11*, 223; (b) Wang, J.; Rustad, J. R.; Casey, W. H. Calculation of Water-Exchange Rates on Aqueous Polynuclear Clusters and at Oxide−Water Interfaces *Inorg. Chem.* **2007**¸ *46*, 2962; (c) Rustad, J. R. Molecular dynamics simulation of the titration of polyoxocations in aqueous solution *Geochim. Cosmochim. Acta* **2005**, *69*, 4397; (d) Rustad, J. R.; Loring, J. S.; Casey, W. H.

Oxygen-exchange pathways in aluminum polyoxocations *Geochim. Cosmochim. Acta* **2004**, *68*, 3011.

25. (a) Villa, E. M.; Ohlin, C. A.; Casey, W. H. Oxygen-Isotope Exchange Rates for Three Isostructural Polyoxometalate Ions *J. Am. Chem. Soc.* **2010**, *132*, 5264; (b) Villa, E. M.; Ohlin, C. A.; Rustad, J. R.; Casey, W. H. Isotope-Exchange Dynamics in Isostructural Decametalates with Profound Differences in Reactivity *J. Am. Chem. Soc.* **2009**, *131*, 16488; (c) Villa, E. M.; Ohlin, C. A.; Balogh, E.; Anderson, T. M.; Nyman, M. D.; Casey, W. H. Reaction Dynamics of the Decaniobate Ion $[H_xNb_{10}O_{28}]^{(6-x)-}$ in Water *Angew. Chem. Int. Ed.* **2008**, *47*, 4844.

26. Gaussian 09, Revision A.1, Frisch, M. J.; Trucks, G. W.; Schlegel, H. B.; Scuseria, G. E.; Robb, M. A.; Cheeseman, J. R.; Scalmani, G.; Barone, V.; Mennucci, B.; Petersson, G. A.; Nakatsuji, H.; Caricato, M.; Li, X.; Hratchian, H. P.; Izmaylov, A. F.; Bloino, J.; Zheng, G.; Sonnenberg, J. L.; Hada, M.; Ehara, M.; Toyota, K.; Fukuda, R.; Hasegawa, J.; Ishida, M.; Nakajima, T.; Honda, Y.; Kitao, O.; Nakai, H.; Vreven, T.; Montgomery, Jr., J. A.; Peralta, J. E.; Ogliaro, F.; Bearpark, M.; Heyd, J. J.; Brothers, E.; Kudin, K. N.; Staroverov, V. N.; Kobayashi, R.; Normand, J.; Raghavachari, K.; Rendell, A.; Burant, J. C.; Iyengar, S. S.; Tomasi, J.; Cossi, M.; Rega, N.; Millam, N. J.; Klene, M.; Knox, J. E.; Cross, J. B.; Bakken, V.; Adamo, C.; Jaramillo, J.; Gomperts, R.; Stratmann, R. E.; Yazyev, O.; Austin, A. J.; Cammi, R.; Pomelli, C.; Ochterski, J. W.; Martin, R. L.; Morokuma, K.; Zakrzewski, V. G.; Voth, G. A.; Salvador, P.; Dannenberg, J. J.; Dapprich, S.; Daniels, A. D.; Farkas, Ö.; Foresman, J. B.; Ortiz, J. V.; Cioslowski, J.; Fox, D. J. Gaussian, Inc., Wallingford CT, 2009.

27. (a) Lee, C.; Yang, C.; Parr, R. G. Development of the Colle-Salvetti correlation-energy formula into a functional of the electron density *Phys. Rev. B* **1988**, *37*, 785. (b) Becke, A. D. A

new mixing of Hartree–Fock and local density functional theories *J. Chem. Phys.* **1993**, *98*, 5648. (c) Stephens, P. J.; Devlin, F. J.; Chabalowski, C. F.; Frisch, M. J. Ab initio calculation of vibrational absorption and circular dichroism spectra using density functional force fields *J. Phys. Chem.* **1994**, *98*, 11623.

28. Hay, P. J.; Wadt, W. R. Ab initio effective core potentials for molecular calculations. Potentials for K to Au including the outermost core orbitals *J. Chem. Phys.* **1985**, *82*, 270.

29. (a) Francl, M. M.; Pietro, W. J.; Hehre, W. J.; Binkley, J. S.; Gordon, M. S.; Defrees, D. J.; Pople, J. A. Self-consistent molecular orbital methods. XXIII. A polarization-type basis set for second-row elements *J. Chem. Phys.* **1982**, *77*, 3654; (b) Hehre, W. J.; Ditchfield, R.; Pople, J. A. Self—consistent molecular orbital methods. XII. Further extensions of gaussian—type basis sets for use in molecular orbital studies of organic molecules *J. Chem. Phys.* **1972**, *56*, 2257; (c) Hariharan, P. C.; Pople, J. A. The influence of polarization functions on molecular orbital hydrogenation energies *Theor. Chim. Acta* **1973**, *28*, 213.

30. Cances, E.; Mennucci, B.; Tomasi, J. A new integral equation formalism for the polarizable continuum model: Theoretical background and applications to isotropic and anisotropic dielectrics *J. Chem. Phys.* **1997**, *107*, 3032.

31. (a) Antonova, N. S.; Carbó, J. J.; Kortz, U.; Kholdeeva, O. A.; Poblet, J. M. Mechanistic Insights into Alkene Epoxidation with H_2O_2 by Ti- and other TM-Containing Polyoxometalates: Role of the Metal Nature and Coordination Environment *J. Am. Chem. Soc*. **2010**, *132*, 7488; (b) Donoeva, B. G.; Trubitsina, T. A.; Antonova, N. S.; Carbó, J. J.; Poblet, J. M.; Al-Kadamany, G.; Kortz, U.; Kholdeeva, O. A. Epoxidation of Alkenes with H2O2 Catalyzed by Dititanium-Containing 19-Tungstodiarsenate(III): Experimental and Theoretical Studies *Eur. J. Inorg.*

Chem. **2010**, 5312; (c) Aguado-Ullate, S.; Carbó, J. J.; González-del Moral, O.; Martín, A.; Mena, M.; Poblet, J. M.; Santamaría, C. Ammonia Activation by μ3-Alkylidyne Fragments Supported on a Titanium Molecular Oxide Model *Inorg. Chem.*, **2011**, *50*, 6269; (d) Jiménez-Lozano, P.; Ivanchikova, I. D.; Kholdeeva, O. A.; Poblet, J. M.; Carbó, J. J. Alkene oxidation by Ti-containing polyoxometalates. Unambiguous characterization of the role of the protonation state *Chem. Commun.* **2012**, *48*, 9266; (e) Skobelev, I. Y.; Zalomaeva, O. V.; Kholdeeva, O. A.; Poblet, J. M.; Carbó, J. J. Mechanism of Thioether Oxidation over Di-and Tetrameric Ti Centres: Kinetic and DFT Studies Based on Model Ti-Containing Polyoxometalates *Chem. Eur. J.* **2015**, *21*, 14496; (f) Jiménez-Lozano, P.; Skobelev, I. Y. ; Kholdeeva, O. A.; Poblet, J. M.; Carbó, J. J. Alkene Epoxidation Catalyzed by Ti-Containing Polyoxometalates: Unprecedented β-Oxygen Transfer Mechanism *Inorg. Chem.* **2016**, 55, 6080.

32. Mammer, M., Shakhnovich, E. I., Deutch, J. M., Whitesides, G. M. Estimating the Entropic Cost of Self-Assembly of Multiparticle Hydrogen-Bonded Aggregates Based on the Cyanuric Acid·Melamine Lattice *J. Org. Chem.* **1998**, *63*, 3821.

33. (a) Ishikawa, A.; Nakao, Y.; Sato, H.; Sakaki, S. Oxygen Atom Transfer Reactions of Iridium and Osmium Complexes: Theoretical Study of Characteristic Features and Significantly Large Differences Between These Two Complexes *Inorg. Chem*. **2009**, *48*, 8154; (b) Zeng, G.; Sakaki, S. Noble Reaction Features of Bromoborane in Oxidative Addition of B–Br σ-Bond to $[M(PMe_3)_2]$ (M = Pt or Pd): Theoretical Study *Inorg. Chem*. **2011**, *50*, 5290; (c) Zeng, G.; Sakaki, S. Theoretical Study on the Transition-Metal Oxoboryl Complex: M–BO Bonding Nature, Mechanism of the Formation Reaction, and Prediction of a New Oxoboryl Complex *Inorg. Chem*. **2012**, *51*, 4597: (d) Aono, S.; Sakaki, S. Evaluation Procedure of Electrostatic Potential in 3D-RISM-SCF Method and Its Application to Hydrolyses of Cis- and Transplatin

Complexes *J. Phys. Chem. B* **2012**, *116*, 13045; (e) Zeng, G.; Sakaki, S.; Fujita, K.; Sano, H.; Yamaguchi, R. Efficient Catalyst for Acceptorless Alcohol Dehydrogenation: Interplay of Theoretical and Experimental Studies *ACS Catal*. **2014**, *4*, 1010.

34. Hodgman, C. D.; *Handbook of Chemistry and Physics*, (39th Ed.), Chemical Rubber Publishing, Cleveland, (1957), p. 1993.

35. Perkins, S. J. Protein volumes and hydration effects *Eur. J. Biochem*. **1986**, *157*, 169.

36. AMBER 11: Case, D. A.; Darden, T. A.; Cheatham, T.E.; Simmerling, C. L.; Wang, J.; Duke, R. E.; Luo, R.; Walker, R.C.; Zhang, W.; Merz, K.M.; Roberts, B.; Wang, B.; Hayik, S.; Roitberg, A.; Seabra, G.; Kolossvai, I.; Wong, K. F.; Paesani, F.; Vanicek, J.; Liu, J.; Wu, X.; Brozell, S. R.; Steinbrecher, T.; Gohlke, H.; Cai, Q.; Ye, X.; Wang, J.; Hsieh, M. J.; Cui, G.; Roe, D. R.; Mathews, D. H.; Seetin, M. G.; Sagui, C.; Babin, V.; Luchko, T.; Gusarov, S.; Kovalenko, A.; Kollman, P. A., University of California, San Francisco, 2010.

37. Solé-Daura, A.; Goovaerts, V.; Stroobants, K.; Absillis, G.; Jiménez-Lozano, P.; Poblet, J. M.; Hirst, J. D.; Parac-Vogt, T. N.; Carbó, J. J. Probing Polyoxometalate–Protein Interactions Using Molecular Dynamics Simulations *Chem. Eur. J*. **2016**, *22*, 15280.

38. (a) López, X.; Nieto-Draghi, C.; Bo, C.; Bonet-Avalos, J.; Poblet, J. M. Polyoxometalates in Solution: Molecular Dynamics Simulations on the α-$PW_{12}O_{40}^{3-}$ Keggin Anion in Aqueous Media *J. Phys. Chem. A* **2005**, *109*, 1216; (b) Leroy, F.; Miró, P.; Poblet, J. M.; Bo, C.; Bonet-Ávalos, J. Keggin polyoxoanions in aqueous solution: ion pairing and its effect on dynamic properties by molecular dynamics simulations *J. Phys. Chem. B*, 2008, **112**, 8591.

39. W Jorgensen, W. L.; Chandrasekhar, J.; Madura, J. D.; Impey, R. W.; Klein, M. L. Comparison of simple potential functions for simulating liquid water *J. Chem. Phys.* **1983**, 79, 926.

40. Darden, T. A.; York, D. M.; Pedersen, L. G. Particle mesh Ewald: An N· log (N) method for Ewald sums in large systems *J. Chem. Phys.* **1993,** 98, 10089.

41. Berendsen, H. J. C.; Postma, J. P. M.; van Gunsteren W. F.; DiNola, A. Molecular dynamics with coupling to an external bath *J. Chem. Phys*., **1984**, *81*, 3684.

42. Hockney, R. W.; Goel, S. P.; Eastwood, J.; Quiet, J. Quiet high-resolution computer models of a plasma *J. Comp. Phys*., **1974**, *14*, 148.

43. *CPMD*, IBM Corp., Armonk, NY, **1990**–**2006**; MPI für Festkörperforschung, Stuttgart, **1997**–**2001**.

44. Troullier, N.; Martins, J. L. Efficient pseudopotentials for plane-wave calculations *Phys. Rev. B* **1991,** *43*, 1993.

45. Louie, S. G.; Froyen, S.; Cohen, M. L. Nonlinear ionic pseudopotentials in spin-density-functional calculations *Phys. Rev. B* **1982**, *26*, 1738.

46. Becke, A. D. Density-functional exchange-energy approximation with correct asymptotic behavior *Phys. Rev. A.* **1988**, *38*, 3098.

47. Bühl, M.; Parrinello, M. Medium Effects on ^{51}V NMR Chemical Shifts: A Density Functional Study *Chem. Eur. J.* **2001**, *7*, 4487.

48. (a) Nosé, S. A unified formulation of the constant temperature molecular dynamics methods *J. Chem. Phys.* **1984**, *81*, 511; (b) Hoover, W. G. Canonical dynamics: equilibrium phase-space distributions *Phys. Rev. A* **1985**, *31*, 1695.

49. Note that for the steps without change in their molecularity the "standard" ΔG and the ΔG corrected with Whitesides' approach have the same value

For Table of Contents only.

The assembly mechanism of Zr- and other transition metal-substituted polyoxometalates (POMs) to form covalently linked dimers has been analyzed by means of static density functional theory (DFT) and Car-Parrinello molecular dynamics (CPMD) simulations. The study identifies the Zr-aqua-hydro anion, $[W_5O_{18}Zr(OH)(H_2O)]^{3-}$, as the active species at basic conditions. For $[W_5O_{18}TM(H_2O)_m(OH)]^{n-}$ anions, the energy barrier is low for Zr^{IV} as a consequence of the flexible coordination environment, moderate for Ti^{IV}, and high for W^{VI}.